AD-A038 049 HARRY DIAMOND LABS ADELPHI MD F/G 9/5
SIMULATOR FIELDS AND GROUND CONSTANTS.(U)
FEB 77 E MARX
UNCLASSIFIED HDL-TR-1785 NL

1 OF 1
ADA038049

END

DATE FILMED
4-77

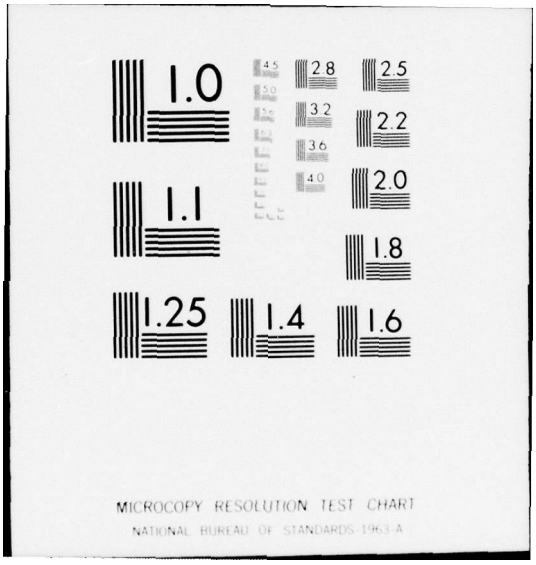
1.0
1.1
1.25
1.4
1.6
1.8
2.0
2.2
2.5
2.8
3.2
3.6
4.0
4.5
5.0
5.6
MICROCOPY RESOLUTION TEST CHART
NATIONAL BUREAU OF STANDARDS-1963-A

HDL-TR-1755

Simulator Fields and Ground Constants

February 1977

U.S. Army Material Development
and Readiness Command
HARRY DIAMOND LABORATORIES
Adelphi, Maryland 20783

UNCLASSIFIED
SECURITY CLASSIFICATION OF THIS PAGE (When Data Entered)

REPORT DOCUMENTATION PAGE		READ INSTRUCTIONS BEFORE COMPLETING FORM
1. REPORT NUMBER HDL-TR-1785	2. GOVT ACCESSION NO.	3. RECIPIENT'S CATALOG NUMBER
4. TITLE (and Subtitle) Simulator Fields and Ground Constants		5. TYPE OF REPORT & PERIOD COVERED Technical Report
		6. PERFORMING ORG. REPORT NUMBER
7. AUTHOR(s) Egon Marx		8. CONTRACT OR GRANT NUMBER(s) DA: 1W162118AH75
9. PERFORMING ORGANIZATION NAME AND ADDRESS Harry Diamond Laboratories 2800 Powder Mill Road Adelphi, MD 20783		10. PROGRAM ELEMENT, PROJECT, TASK AREA & WORK UNIT NUMBERS Program: 6.21.18A
11. CONTROLLING OFFICE NAME AND ADDRESS U.S. Army Materiel Development and Readiness Command Alexandria, VA 22333		12. REPORT DATE February 1977 13. NUMBER OF PAGES 32
14. MONITORING AGENCY NAME & ADDRESS(if different from Controlling Office) 28 p.		15. SECURITY CLASS. (of this report) UNCLASSIFIED 15a. DECLASSIFICATION/DOWNGRADING SCHEDULE

16. DISTRIBUTION STATEMENT (of this Report)

Approved for public release; distribution unlimited.

17. DISTRIBUTION STATEMENT (of the abstract entered in Block 20, if different from Report)

18. SUPPLEMENTARY NOTES

HDL Project: X756E2
DRCMS Code: 61211811H7500
This work was funded under DARCOM NWER/T Program Element 6.21.18A, titled Multiple Systems Evaluation Program.

19. KEY WORDS (Continue on reverse side if necessary and identify by block number)

Electromagnetic pulse
Ground reflection
Ground parameters

20. ABSTRACT (Continue on reverse side if necessary and identify by block number)

The consistency of field measurements and the determination of ground constants is examined for electromagnetic pulse (EMP) simulators, such as the Transportable Electromagnetic Pulse Simulator (TEMPS) and the Army EMP Simulator Operation (AESOP). The agreement between the horizontal electric field and the radial magnetic field is quite good for reasonable values of the ground constants. More refined measurements of the fields can lead to a more precise determination of the conductivity and dielectric

DD FORM 1 JAN 73 1473 EDITION OF 1 NOV 65 IS OBSOLETE

constant of the ground and even to show the frequency dependence of these parameters.

As part of the Multiple Systems Evaluation Program, considerable testing has been performed using EMP simulators such as AESOP. To better understand the response of Army equipment both to simulators and to EMP, the tester must study the effects of ground parameters on these waves. An additional benefit of this effort is that it allows for independent validation of the field-sensing equipment employed.

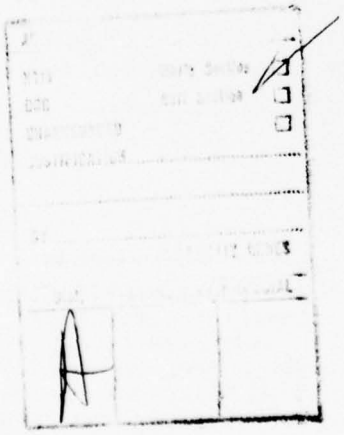

CONTENTS

FIGURES

FIGURES (Cont'd)

1. INTRODUCTION

The problem considered in this report concerns the relationship between components of the measured fields due to an electromagnetic pulse (EMP) simulator and the possibility of extracting information about the conductivity and permittivity of the ground.

Radiation fields emitted by a pulser can locally be approximated by plane waves, and the monochromatic components of the incident and reflected pulses are related by Fresnel's coefficients. These coefficients involve the ground parameters; when they are known, the free field can be computed from the resultant fields in the air. Alternatively, two measurements of different fields for the same pulse can be compared for different values of the parameters until agreement is found.

Simulators such as the Transportable Electromagnetic Pulse Simulator (TEMPS) and the Army EMP Simulator Operation (AESOP) produce mainly horizontally polarized fields, especially on the center line (see fig. 1). For these fields, the reflected electric field is almost 180 deg out of phase with the incident field, and the peak of the resultant field is determined mostly by the delay time, returning quickly to zero after that. The vertical component of the resultant magnetic field is strictly proportional to the electric field. Simultaneous measurements of these two fields can be used to determine that the respective probes produce traces that are in agreement with each other. The horizontal component of the magnetic field is proportional to the difference (essentially the sum of the magnitudes) between the incident and reflected fields and shows much more detail of the incident pulse. This component can be used to determine the free field and then the resultant electric field, by using the Fresnel coefficient. When the correct values of the ground conductivity and dielectric constant are used, this procedure serves to verify both the

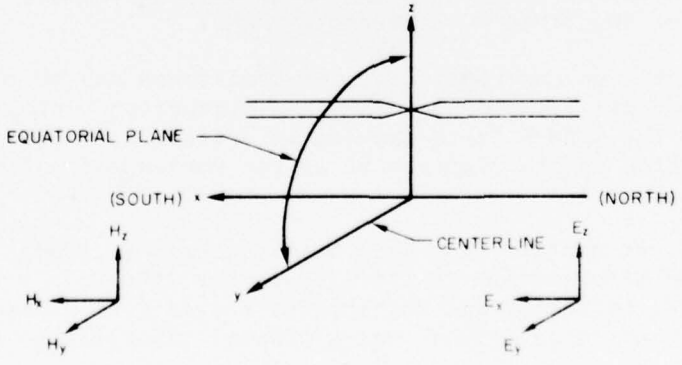

Figure 1. The TEMPS coordinate system.

ground parameters and the agreement of the probes. Furthermore, precise measurements of the field would allow a determination of the frequency dependence of the ground parameters.

Two sets of field measurements were used in this work. One was taken with the sensor box on the ground; the other, at a height of 5 m. The quality of the photographs was acceptable, but much improvement is needed.

The electric field was computed from the radial magnetic field, and this curve was compared to the measured electric field. The corresponding spectra also were compared. The values of the ground parameters were varied to find what effect they have on the agreement between both sets of curves, and reasonable values of the parameters were found that produced acceptable matching of the curves. Other input parameters, such as the height and the calibration constants of the probe, were varied, but no significant improvement was found to justify such a change.

A somewhat different way of comparing the curves also is presented, and it should be tried in future work. It could avoid some difficulties with the numerical computations.

Similar considerations are valid for "vertical" polarization. The vertical component of the resultant electric field and the horizontal magnetic field are proportional to each other, and they can be used to compute the radial component of the electric field. Field mapping has shown that the electric field produced by the TEMPS has a sizable vertical component off the center line.

Once this procedure is well established, it can be used to map the ground parameters at a given site and to observe their variation with the water content and other local changes. More refined measurements also could be used to determine the frequency dependence of the ground parameters for the range of interest for EMP.

Information on numerical Fourier transforms can be found,[1] and the theory of pulses incident on a conducting ground has been published.[2] The TEMPS field mapping is available,[3] and details about the digitization of the traces will be the subject of a future report by Thomas V. Noon.

---

[1] *Alfred G. Brandstein and Egon Marx, Numerical Fourier Transform, Harry Diamond Laboratories TR-1748 (September 1976).*

[2] *Egon Marx, Reflected and Transmitted Fields for a Plane-wave Pulse Incident on Conducting Ground, Harry Diamond Laboratories TR-1740 (April 1976).*

[3] *E. Patrick and S. Soo Hoo, Transportable Electromagnetic Pulse Simulator (TEMPS) Preliminary Field Mapping Report, Harry Diamond Laboratories TM-74-15 (October 1974).*

2. FIELD COMPONENTS

An EMP simulator, such as the TEMPS or AESOP, produces a pulse that on the center line is horizontally polarized to a good degree of approximation. Locally, the fields correspond to those of a plane wave, and Fresnel's formulas can be used to determine the reflected wave. The ground is assumed to be plane and homogeneous.

To determine the reflected field, the incident field is decomposed into its Fourier components,

$$E(t) = \frac{1}{2\pi} \int_{-\infty}^{\infty} E_\omega e^{i\omega t} d\omega \quad ; \tag{1}$$

then the reflected field is obtained from

$$E'(t) = \frac{1}{2\pi} \int_{-\infty}^{\infty} E_\omega R_h(\omega) e^{i\omega t} d\omega \ , \tag{2}$$

where the Fresnel coefficient for horizontal polarization is

$$R_h = \frac{\sin\psi - \left[\kappa - i\left(\sigma/\varepsilon_o\omega\right) - \cos^2\psi\right]^{\frac{1}{2}}}{\sin\psi + \left[\kappa - i\left(\sigma/\varepsilon_o\omega\right) - \cos^2\psi\right]^{\frac{1}{2}}} \ . \tag{3}$$

The total field in the air at height h is then given by

$$E_y(t) = E_h(t) + E_h'\left(t - t_D\right) \ , \tag{4}$$

where the time delay is

$$t_D = 2h \sin\psi/c \ . \tag{5}$$

The magnetic field of each pulse is perpendicular to the electric field, and the vertical and horizontal components are

$$H_x(t) = Z_o^{-1}\left[E_h(t) - E_h'\left(t - t_D\right)\right]\sin\psi \ , \tag{6}$$

$$H_z(t) = Z_o^{-1}\left[E_h(t) + E_h'\left(t - t_D\right)\right]\cos\psi \ , \tag{7}$$

where

$$Z_o = \left(\mu_o/\varepsilon_o\right)^{\frac{1}{2}} . \tag{8}$$

Thus, the vertical component of the magnetic field is proportional to the electric field. For a perfect conductor, $R_h = -1$, and these components follow the free field until time t_D and then rapidly return to zero, due to the cancellation of the fields of the incident and reflected pulses. On the other hand, the horizontal component of the magnetic field is proportional to the delayed sum of the two pulses and approximates the shape of the free field when the time delay is small.

The Fourier transform of the horizontal component of the magnetic field is

$$H_{x\omega} = Z_o^{-1} \left(1 - R_h e^{-i\omega t_D}\right) \sin \psi \, E_\omega , \tag{9}$$

and the free field can be obtained from the measured H_x. Furthermore,

$$E_{y\omega} = \left(1 + R_h e^{-i\omega t_D}\right) E_\omega \tag{10}$$

also can be computed, and its Fourier transform should reproduce the measured electric field.

3. FIELD MEASUREMENTS

Two sets of measurements were taken for this report. They consisted of simultaneous measurements of E_x and H_y with different faces of the same Stanford Research Institute dome-type sensor box. Different sweep speeds were recorded during separate shots; that is, only two pictures were obtained from each shot. The measurements were taken on the center line, at 100 m from the simulator. The first set was obtained from a sensor on the ground with AESOP; the second set, at a height of 5 m with the TEMPS pulser in the AESOP frame.

The time-amplitude traces are shown in figures 2 to 5. The composite digitized traces of the magnetic field and the frequency spectra are shown in figures 6 to 9.

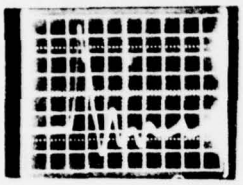

TIME SCALE: 10ns/div
VOLTAGE SCALE: 200mV/div

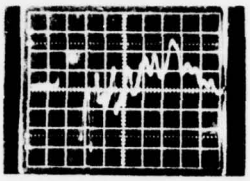

TIME SCALE: 20ns/div
VOLTAGE SCALE: 50mV/div

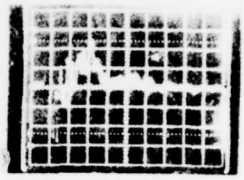

TIME SCALE: 50ns/div
VOLTAGE SCALE: 50mV/div

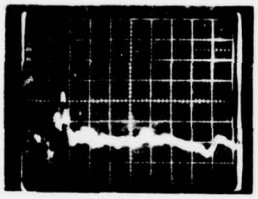

TIME SCALE: 100ns/div
VOLTAGE SCALE: 50mV/div

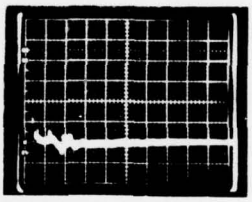

TIME SCALE: 500ns/div
VOLTAGE SCALE: 50mV/div

Figure 2. Time-amplitude traces that form composite trace for horizontal electric field (parallel to Pulser) on center line at 100 m from antenna and with sensor box on ground (sensor height at 0.65 m).

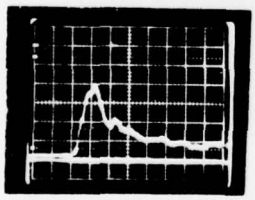

TIME SCALE: 10ns/div
VOLTAGE SCALE: 100mV/div

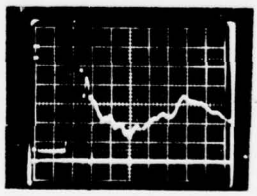

TIME SCALE: 20ns/div
VOLTAGE SCALE: 50mV/div

TIME SCALE: 50ns/div
VOLTAGE SCALE: 20mV/div

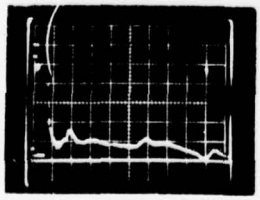

TIME SCALE: 100ns/div
VOLTAGE SCALE: 100mV/div

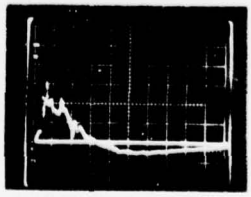

TIME SCALE: 500ns/div
VOLTAGE SCALE: 50mV/div

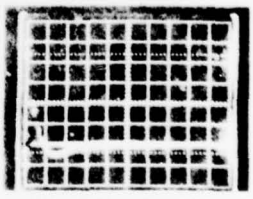

TIME SCALE: 2 μs/div
VOLTAGE SCALE: 50mV/div

Figure 3. Time-amplitude traces for horizontal (radial) magnetic field at 100 m on ground.

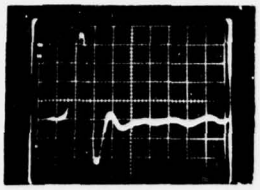

TIME SCALE: 10 ns/div
VOLTAGE SCALE: 100 mV/div

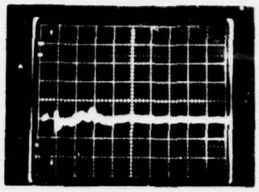

TIME SCALE: 50 ns/div
VOLTAGE SCALE: 100 mV/div

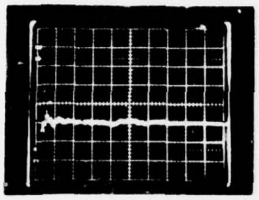

TIME SCALE: 200 ns/div
VOLTAGE SCALE: 50 mV/div

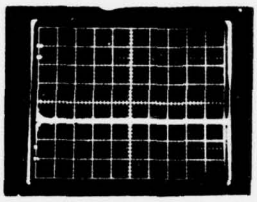

TIME SCALE: 1 μs/div
VOLTAGE SCALE: 50 mV/div

igure 4. Time-amplitude traces for horizontal electric field at 100 m with sensor 5 m aboveground.

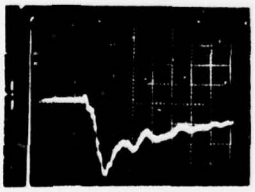

TIME SCALE: 10 ns/div
VOLTAGE SCALE: 100 mV/div

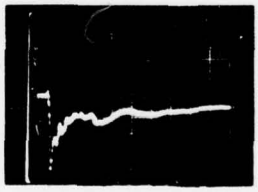

TIME SCALE: 50 ns/div
VOLTAGE SCALE: 100 mV/div

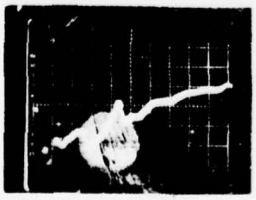

TIME SCALE: 200 ns/div
VOLTAGE SCALE: 50 mV/div

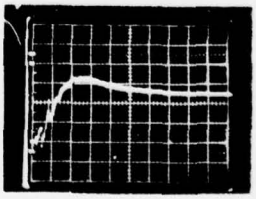

TIME SCALE: 1 μs/div
VOLTAGE SCALE: 50 mV/div

.gure 5. Time-amplitude traces for horizontal magnetic field at 100 m 5 m aboveground.

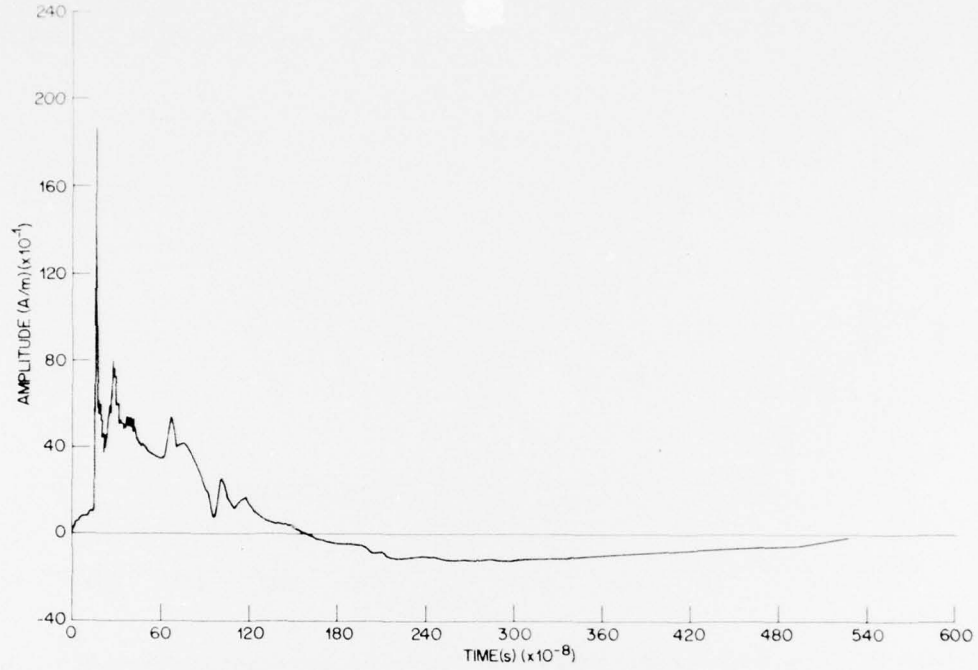

Figure 6. Composite time-amplitude trace of horizontal magnetic field on ground.

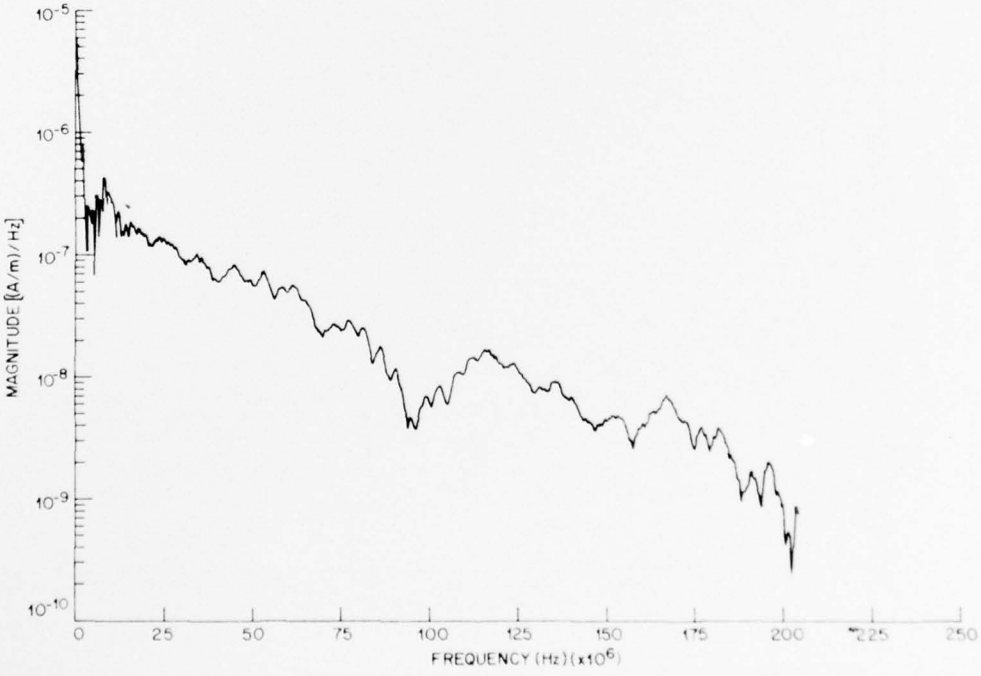

Figure 7. Frequency spectrum of horizontal magnetic field on ground.

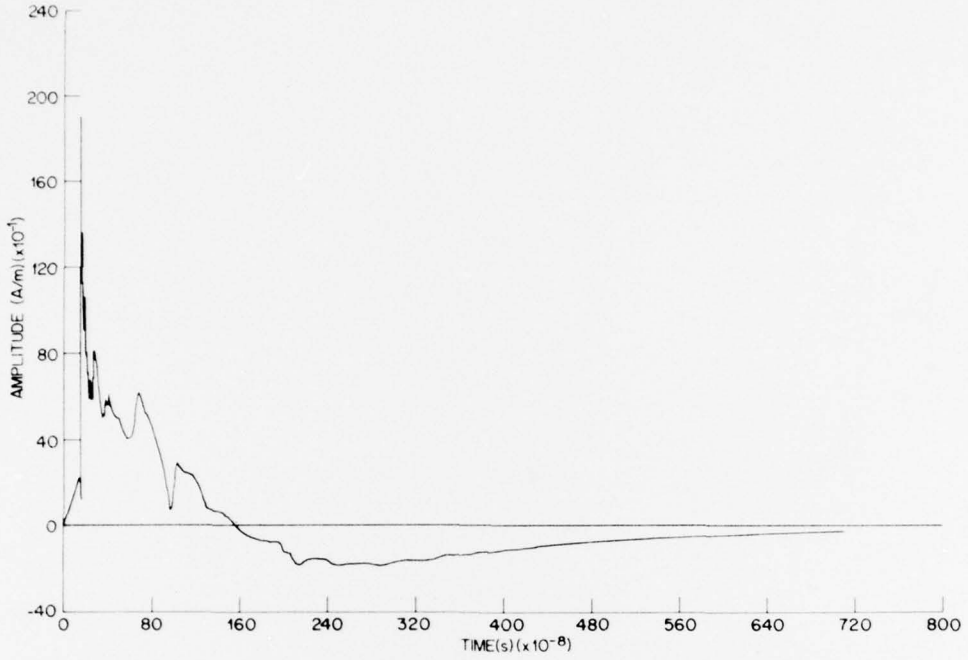

Figure 8. Composite time-amplitude trace of horizontal magnetic field 5 m aboveground.

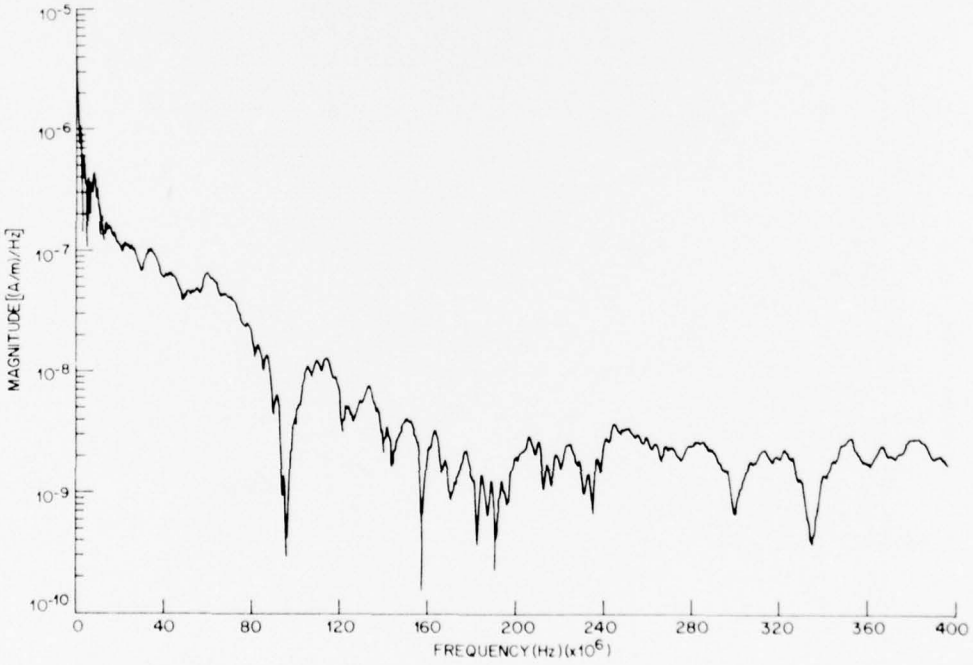

Figure 9. Frequency spectrum of horizontal magnetic field 5 m aboveground.

4. NUMERICAL PROCEDURES

For use as input to the computer program, the time-amplitude traces have to be digitized. Each trace is digitized separately, and a computer program, TRANS, developed by Thomas V. Noon, at the Harry Diamond Laboratories (HDL), gives a single set of coordinates for the entire curve.

Several problems are associated with this procedure. It is assumed that pulses in a set are identical, but they are not really; normally, deviations are small enough so that no severe errors are introduced in this manner. A point has to be identified in each picture that corresponds to the end of the previous trace; this identification is sometimes difficult, but an error that was inadvertently made was discovered through discrepancies in the two curves for the electric field. The ramp that precedes the actual pulse is difficult to obtain for the magnetic field and essentially impossible for the electric field; this ramp was digitized from the third picture in the first set, and it was assumed to be the same for the second set. Another problem related to the ramp is the lack of a precise time when the pulse starts; when comparing the two pulses in the output, one pulse had to be shifted until the leading edges coincided. More generally, the quality of the pictures obtained from the oscilloscopes is such that there is considerable uncertainty in the definition of the points on the digitizer.

Once an acceptable composite trace of the magnetic field was obtained, the points were linearly interpolated to obtain an equispaced set of points suitable for a Fast Fourier Transform (FFT). Then equations (9) and (10) were used to obtain the Fourier transform of the electric field, and an inverse FFT produced a computed trace for the electric field, which was plotted with the measured field. Since this field goes quickly back to zero, only the initial portion of the trace was considered of interest, and most of the resulting ramp also was eliminated from the plots. Alternatively, the absolute values of the Fourier transforms of the computed and measured electric fields were plotted on a semilog plot either for the full range given by the FFT or for only the initial part.

A decision that has to be made is what the number of interpolated points will be. The number 8192 was chosen, because it samples the curve adequately in the region with the largest density of points when the final time is chosen about the end of the magnetic field pulse, at 7.5 or 10 μs. Doubling or quadrupling this number of points did not introduce any significant change in the resulting trace.

A serious problem that arose was a large oscillation superimposed on the computed trace of the electric field. With the help of William T. Wyatt of HDL, the reason for this oscillation was found to be the division by the factor

$$1 - R_h e^{-i\omega t_D}$$

to obtain the free field. The value of R_h is close to -1, and

$$1 + e^{-i\omega t_D}$$

vanishes whenever

$$\omega t_D = k\pi \ , \ k = 1, 3, 5, \ . \ . \ . \ , \tag{11}$$

which causes a peak in the computed E_ω for frequencies close to this value. The numerator, $H_{x\omega}$, also should vanish for these frequencies, but recording, digitization, and computation errors account for the appearance of a large peak in E_ω. Similar computations done for analytic curves (such as a double exponential), displaced in time, show basically the same behavior.

For the box on the ground, the time delay is 0.85 ns, and the first frequency at which this peak occurs is 589 MHz. With 8192 points and a time of 7.5 μs, the significant frequency limit for an FFT is 546 MHz, and this problem barely shows up. On the other hand, for a 5-m height, the time delay is 4.9 ns, and the frequency of the first peak is only 101 MHz.

The solution that was used for this difficulty was a filter function that multiplied E_ω. Several were tried, and the function finally chosen was

$$F(\omega) = \left|\sin \omega t_D / \omega t_D\right|^n \ , \tag{12}$$

which is 1 for small ω and vanishes if ω is given by equation (11). The value $n = 2$ was used for the box on the ground; $n = 1$, for the 5-m height. If this filter is used, the frequency spectrum around the first zero and after that is virtually ignored, due to the ω^{-n} dependence.

Another method that could be tried, especially for a height of 5 m, would be based on the clear time of 4.9 μs to obtain the corresponding reflected field, subtract it from the measured trace, and proceed in this way to obtain the free field. This method was not tried.

It is possible also, following a procedure used by Janis Klebers of HDL, to use equations (4) and (6) to separate the incident and reflected fields,

$$E_h(t) = E_y(t)/2 + Z_o H_x(t)/(2 \sin \psi) , \tag{13}$$

$$E'_h(t - t_D) = -E_y(t)/2 + Z_o H_x(t)/(2 \sin \psi) . \tag{14}$$

Then the matching of the Fresnel coefficient can be done from the Fourier transforms of E_h and E'_h. One difficulty with this approach is the need to know a common initial time for the traces, which knowledge is difficult to get because the ramp is not recorded for the electric field.

5. VARIATION OF PARAMETERS

A number of different parameters can be varied in this computer program. The main concern of this work related to the conductivity of the ground, σ, and the dielectric constant, κ. The height of the sensor also was varied, as were the probe calibration constants, but the measured values were found to be adequate. The angle of incidence was determined from the geometry of the experiment.

A good coincidence of the computed and measured electric fields for the sensor at a height of 0.65 m aboveground was obtained with σ = 20 mmho/m and κ = 25 (fig. 10, 11). Figure 12 shows the full range of the frequency spectrum that is obtained from an 8192-point FFT. There is good agreement in the shape of the Fourier transforms throughout the range, even though the high-frequency end of the computed transform is incorrectly enhanced by the division by

$$1 + R_h e^{-i\omega t_D} .$$

There is an unexplained dip in the transform of the measured electric field at about 280 MHz, where the computed spectrum has a peak. Agreement in the traces is improved by filtering out this frequency, by using

$$F(\omega) = \left(\sin \omega t_1/\omega t_1\right)^{1/2} \left(\sin \omega t_D/\omega t_D\right)^{3/2}, \tag{15}$$

where $t_1 = 1.732 \times 10^{-9}$ s, very nearly twice the time delay.

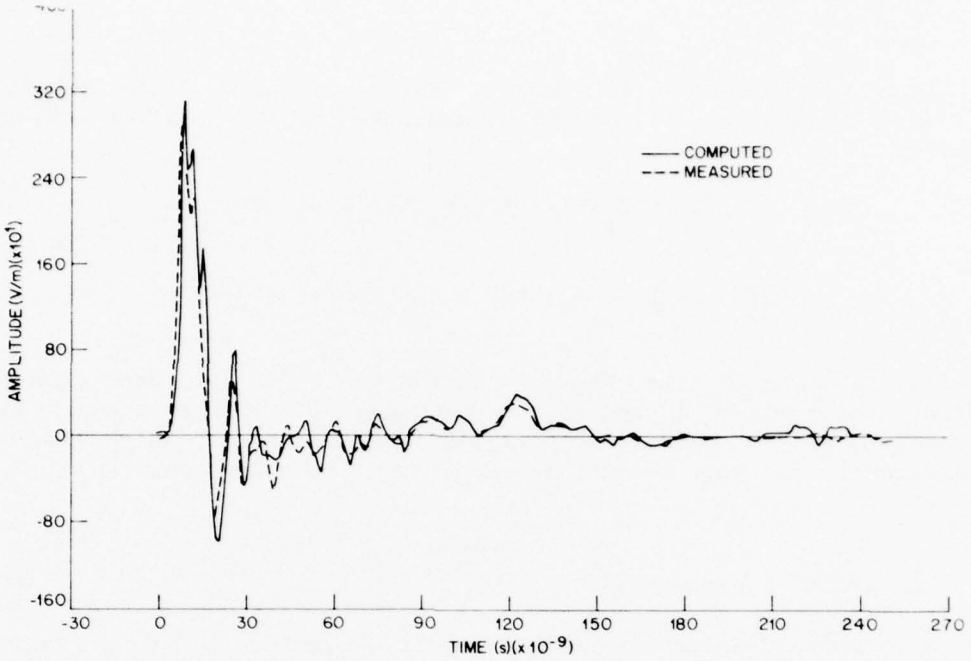

Figure 10. Computed and measured time-amplitude traces of electric field on ground for σ = 20 mmho/m and κ = 25.

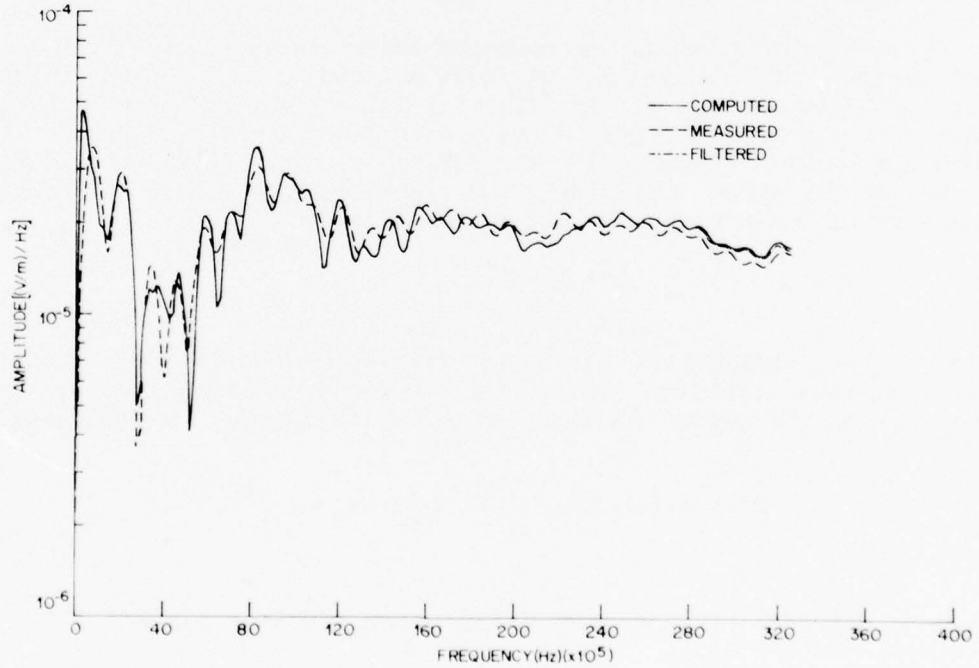

Figure 11. Low-frequency part of spectrum of electric field, as computed from both fields, for σ = 20 mmho/m and κ = 25.

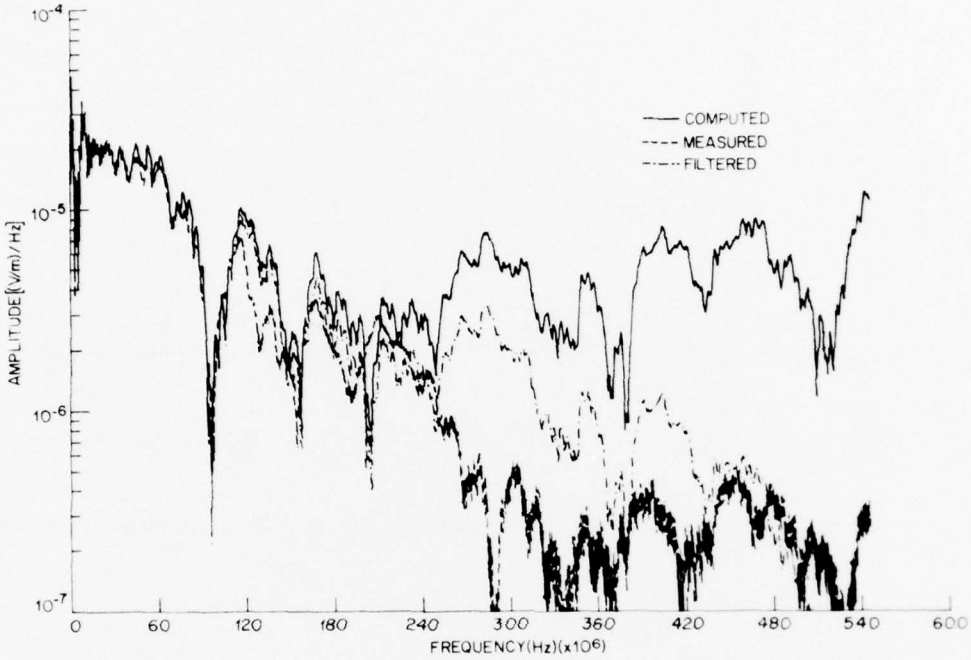

Figure 12. Full range of frequency spectrum as provided by Fast Fourier Transform, for σ = 20 mmho/m and κ = 25.

Figures 13 to 20 show the effects of varying σ and κ to values at the extremes that can be expected for the ground. The conductivity is changed from 0.5 to 100 mmho/m; the dielectric constant, from 1 to 100. The effects of these changes are quite noticeable; the conductivity affects mainly the late times and low frequencies, while the dielectric constant changes mainly the peak of the time-amplitude trace and somewhat higher frequencies.

Figures 21 and 22 show the effects of the change in the assumed height of the sensor aboveground, which through the time delay affects mainly the peak in the time-amplitude trace.

Figure 23 shows the computed trace that is obtained by this method when no filter is used, and figure 24 shows the trace for a 4096-point transform with no filter. The latter is less accurate, but is not affected by the "resonance," because it does not go as high in frequency. Figure 25 shows the effect of the filter in equation (15).

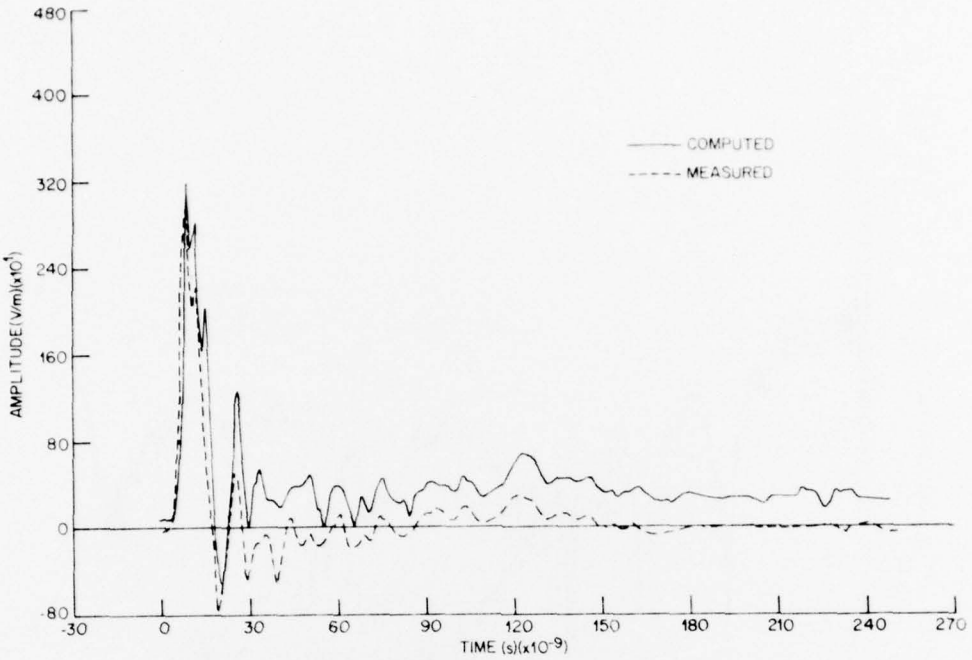

Figure 13. Time-amplitude traces for σ = 0.5 mmho/m, κ = 25.

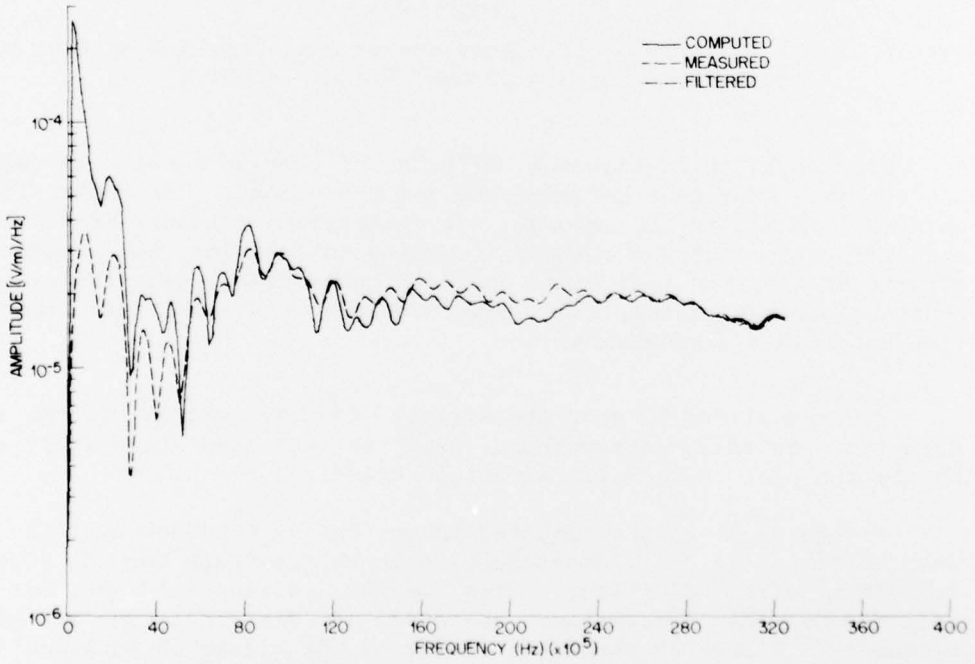

Figure 14. Frequency spectra for σ = 0.5 mmho/m, κ = 25.

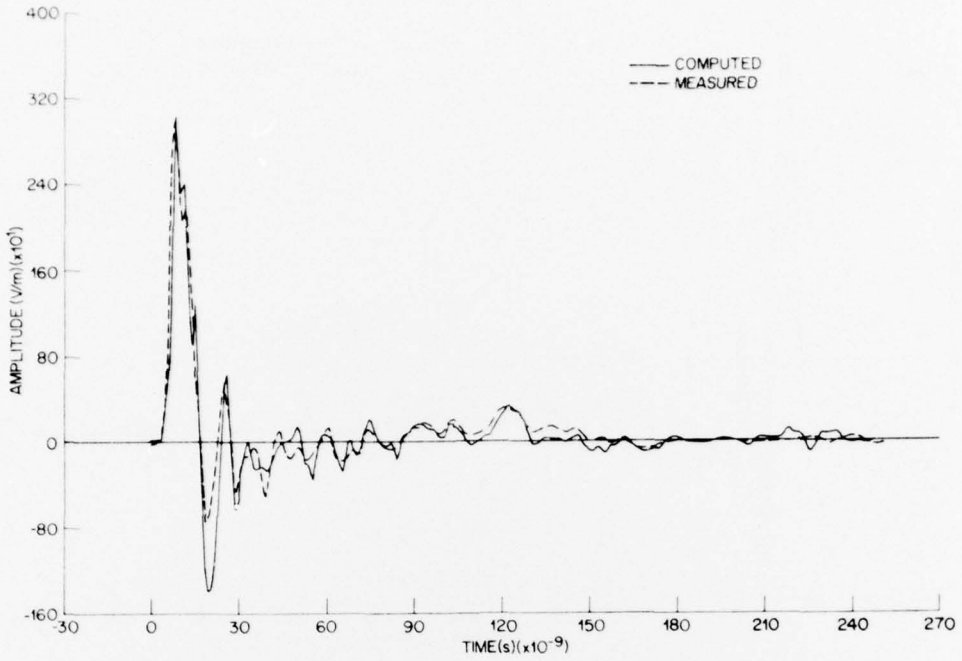

Figure 15. Time-amplitude traces for σ = 100 mmho/m, κ = 25.

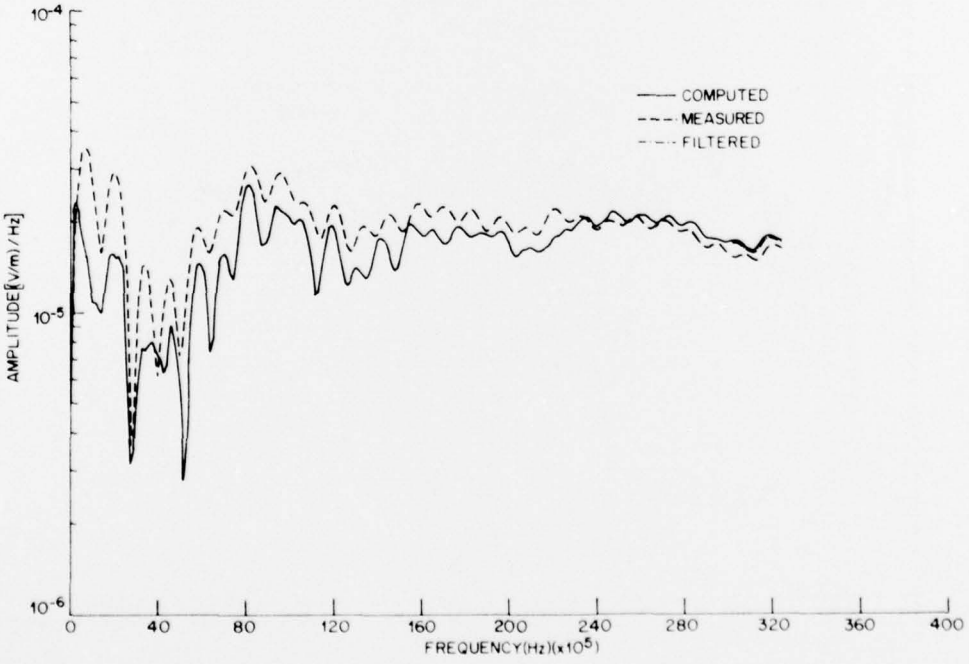

Figure 16. Frequency spectra for σ = 100 mmho/m, κ = 25.

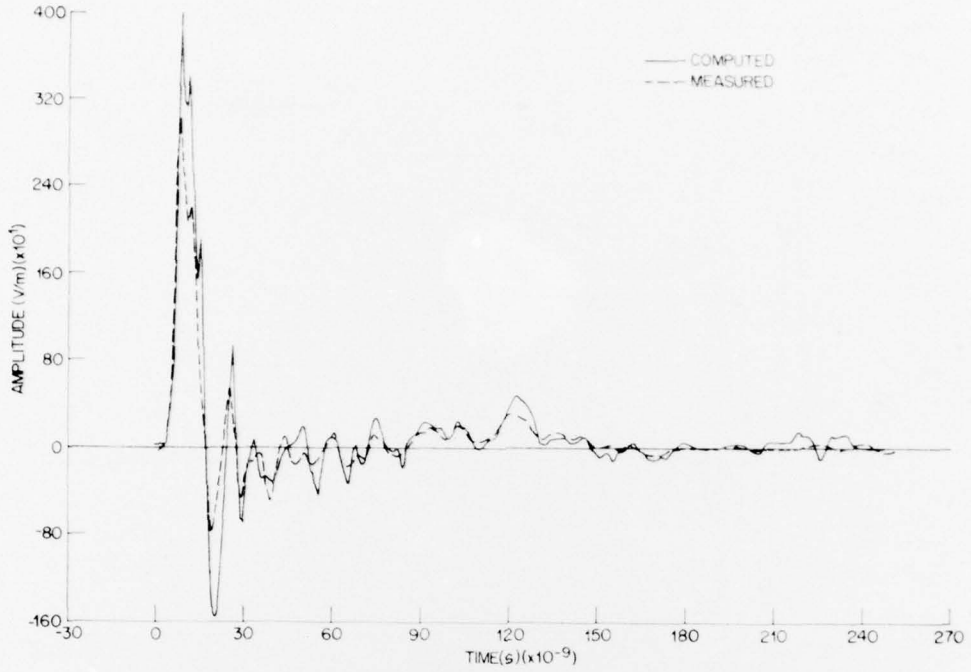

Figure 17. Time-amplitude traces for σ = 20 mmho/m, κ = 1.

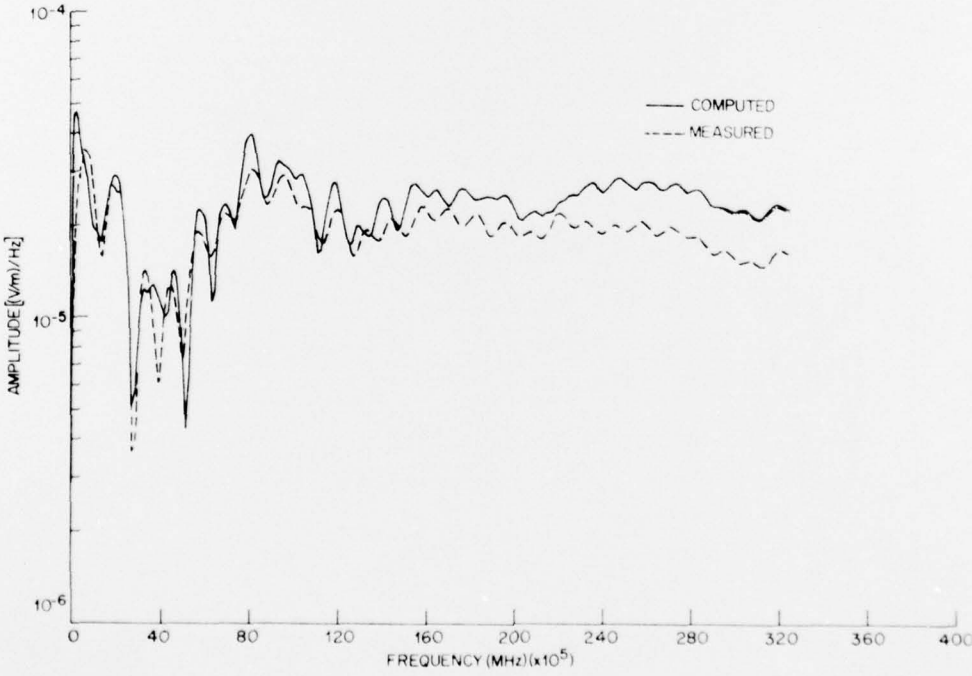

Figure 18. Frequency spectra for σ = 20 mmho/m, κ = 1.

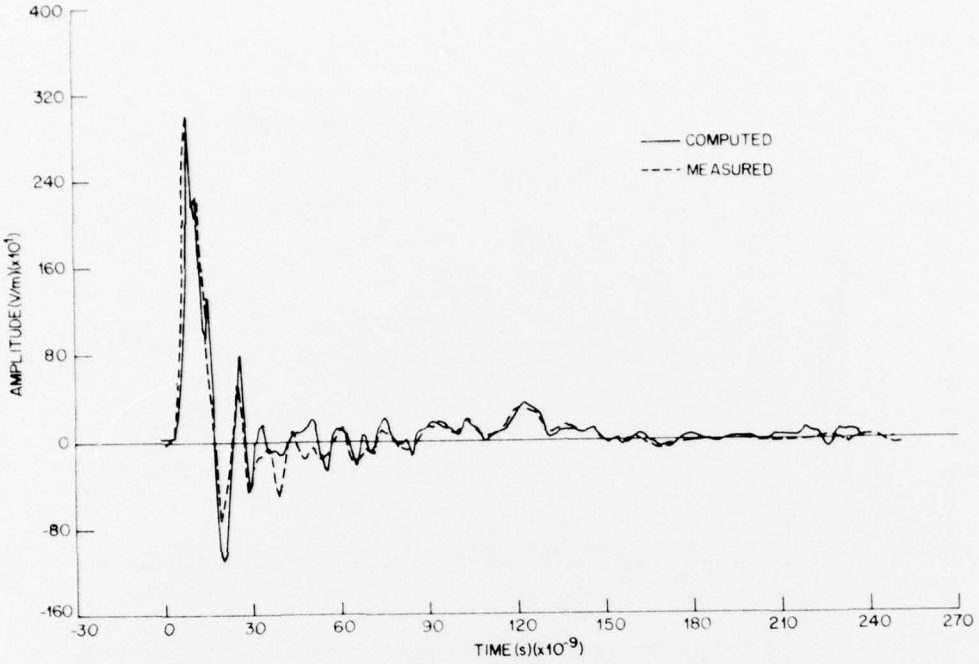

Figure 19. Time-amplitude traces for σ = 20 mmho/m, κ = 100.

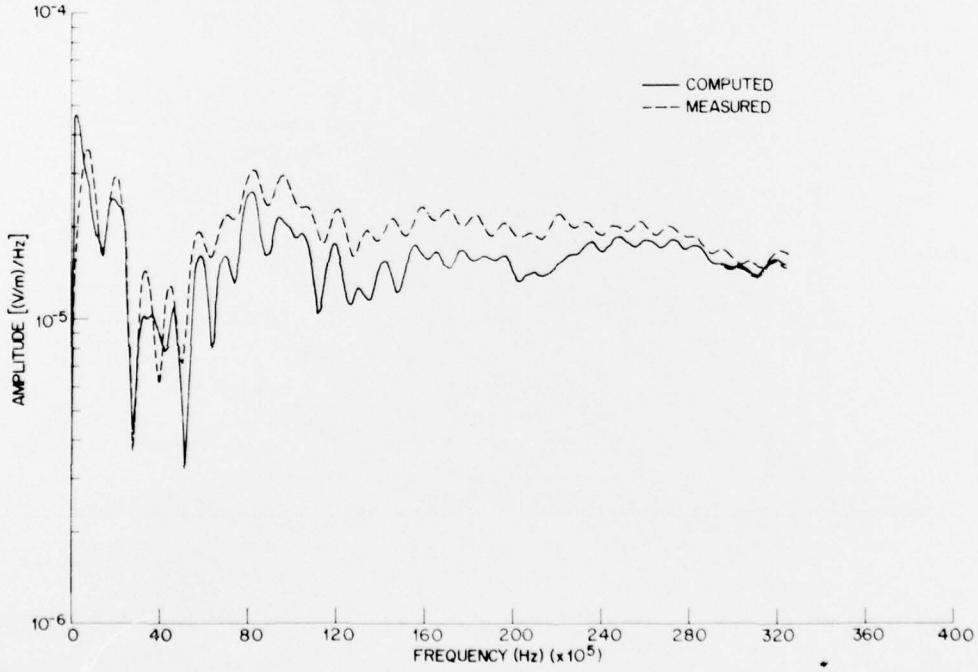

Figure 20. Frequency spectra for σ = 20 mmho/m, κ = 100.

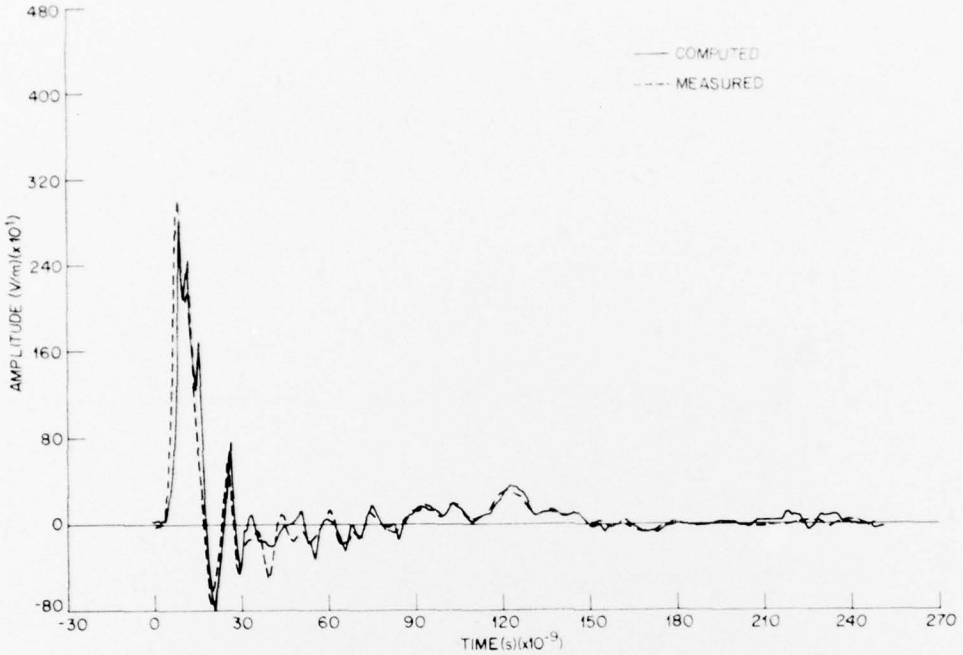

Figure 21. Time-amplitude traces for $\sigma \approx 20$ mmho/m, $\kappa = 25$, assuming that height of sensor aboveground is 0.55 m.

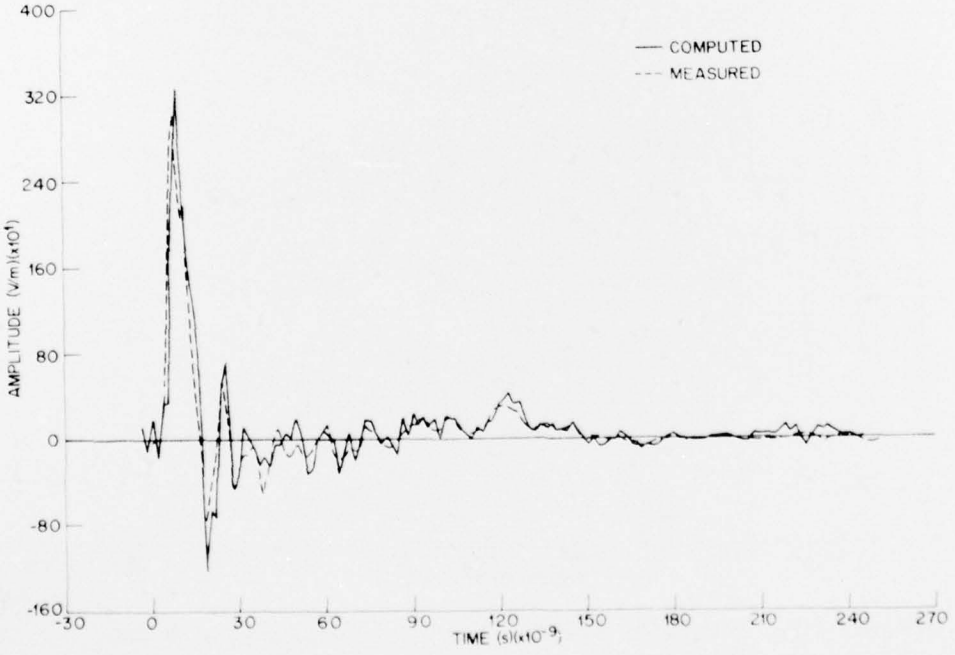

Figure 22. Time-amplitude traces for $\sigma = 20$ mmho/m, $\kappa = 25$, height of sensor aboveground = 0.75 m.

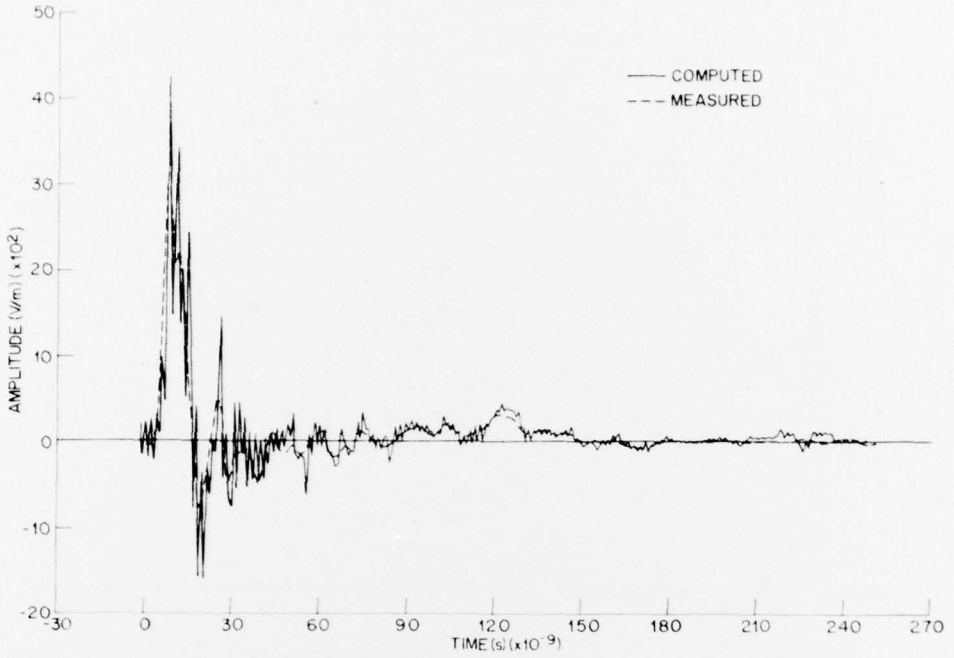

Figure 23. Time-amplitude traces for σ = 20 mmho/m, κ = 25, showing spikes when filter is not used with 8192-point transform.

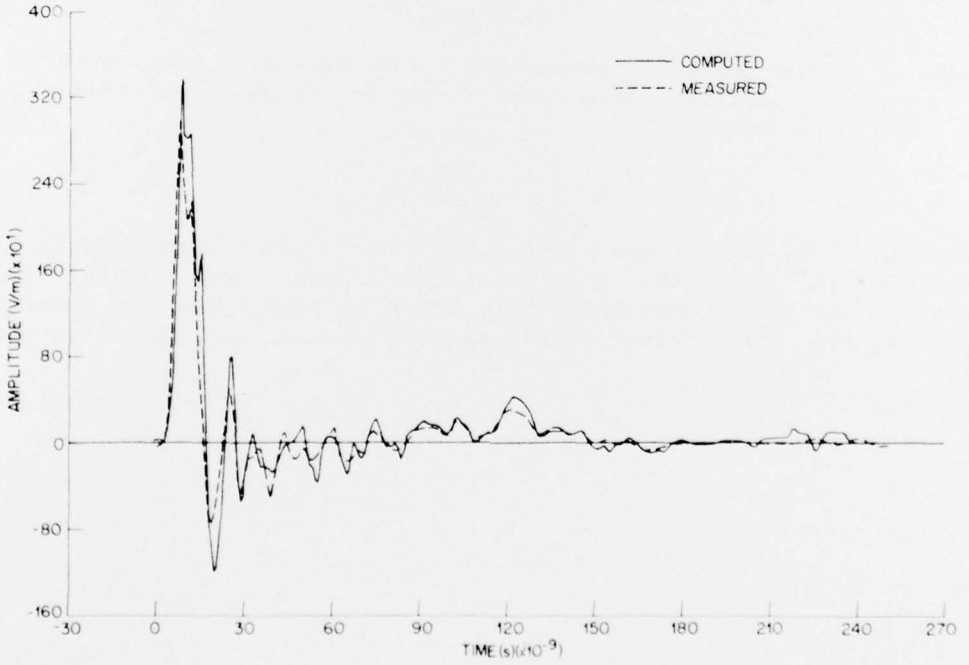

Figure 24. Time-amplitude traces for σ = 20 mmho/m, κ = 25, without filter and with 4096-point transform.

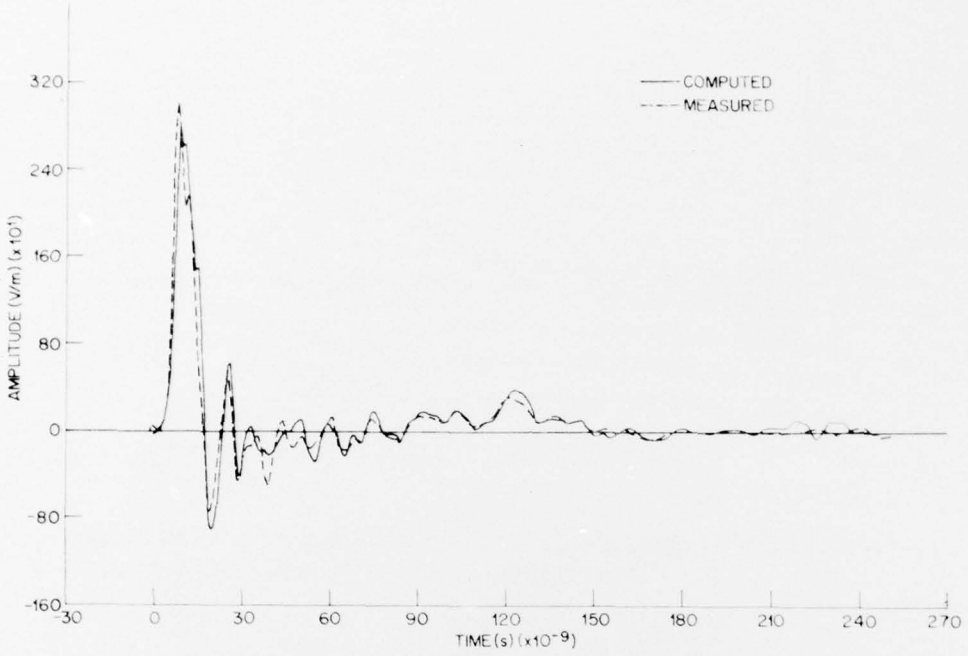

Figure 25. Time-amplitude traces for σ = 20 mmho/m, κ = 25, with filter that corresponds to dip in frequency spectrum at 280 MHz.

Figures 26 to 28 show the same graph for the measurements taken at 5 m aboveground, with the values of σ = 30 mmho/m and κ = 25. The resonance occurs at a correspondingly lower frequency, and the general agreement at low frequencies is not so good as that for the box on the ground.

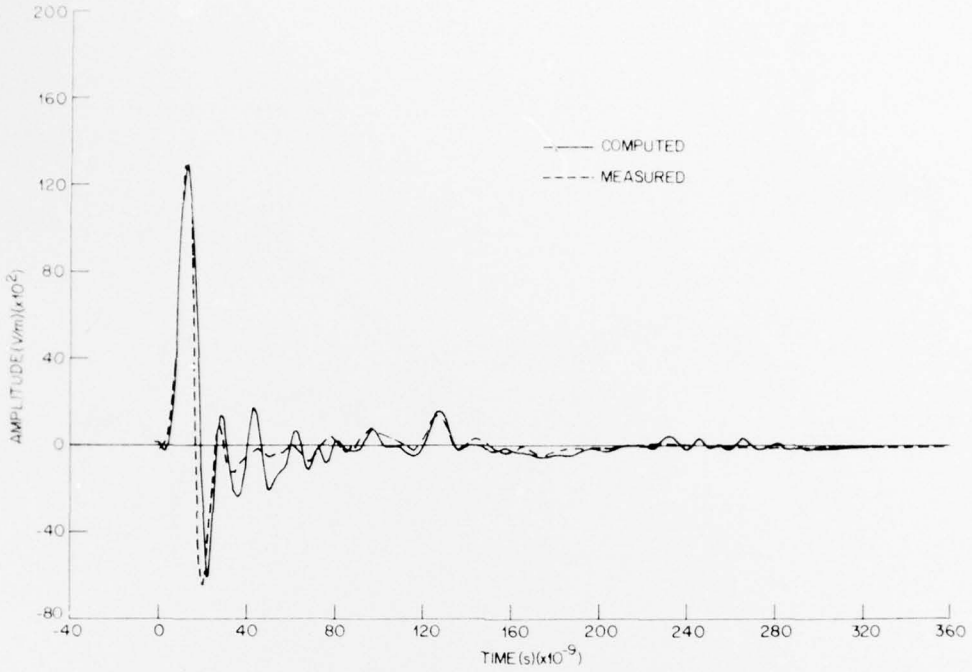

Figure 26. Time-amplitude traces for σ = 30 mmho/m, κ = 25, when measurements are taken with sensors at 5 m aboveground.

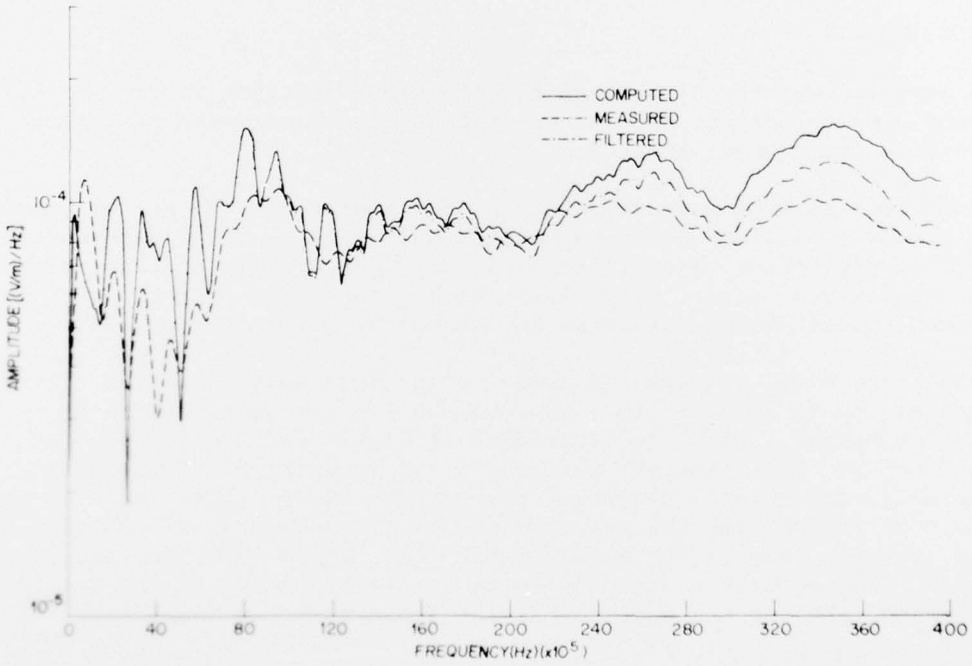

Figure 27. Low-frequency part of spectra for σ = 30 mmho/m, κ = 25, and height of sensor aboveground = 5 m.

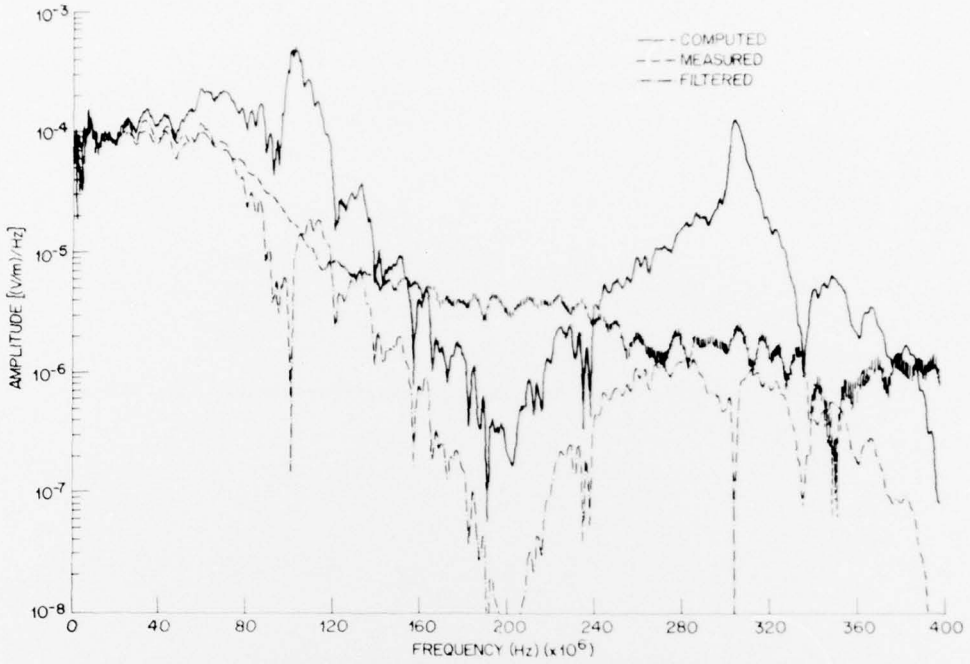

Figure 28. Full range of spectra for σ = 30 mmho/m, κ = 25, and height of sensor aboveground = 5 m.

6. CONCLUSIONS

A good agreement was obtained for the time-amplitude traces and the frequency spectra for the chosen best values of the parameters; however, considerable improvement is needed.

For both sets of measurements, on the ground and at 5 m, the peaks in the electric field could be matched quite well. The agreement was inferior in the following oscillations, to improve again at later times before the field essentially went back to zero. There was no significant qualitative difference in the matching for the two sets.

The frequency spectra showed good agreement also at lower frequencies, up to 200 MHz for the box on the ground and up to 50 MHz for the 5-m height. The wide divergence at higher frequencies was found to be due to the limited accuracy of numerical computations. Surprisingly, the general shapes of the curves agree quite well up to the limit of 550 MHz for the measurements on the ground, except that a dip in the spectrum of the electric field at about 280 MHz was not explained. The quality of the agreement is significantly better for the measurements taken on the ground than for those taken at 5 m.

A number of factors that limited the accuracy of these comparisons can be improved without much difficulty. The different sweep speeds for the oscilloscopes can be taken simultaneously when the instrumentation van is available. The quality of the photographs can be improved to show more detail in rapidly varying portions of the curve and less intensity for the slowly varying parts. The amplifications can be increased to show more detail at late times. Time delays can be used in the triggering circuit to obtain a picture with a high sweep speed at later times, to obtain more detail where necessary. Other numerical techniques can be tried to avoid some of the difficulties with false resonances.

Comparison of the measured and "computed" fields shows that the probes for the electric and magnetic fields agree quite well and are probably accurate in an absolute sense within the range of interest. Also, the calibration constants for the probes were used without modifications, so at least their ratio is correct. The assumptions that the pulse was a plane wave over a homogeneous plane infinite ground in the radiation zone for the field also did not introduce any large errors.

That the wave comes from different parts of the simulator and not from a point source at a large distance might explain some of the discrepancies observed after the first few peaks. Also, the effect of the metal box on the measured field was not taken into account.

In summary, this method provides useful information about the sensors and the ground constants, and it can be extended to fields off the center line and other combinations of components.

DISTRIBUTION

DEFENSE DOCUMENTATION CENTER
CAMERON STATION, BUILDING 5
ALEXANDRIA, VA 22314
ATTN DDC-TCA (12 COPIES)

COMMANDER
US ARMY MATERIEL DEVELOPMENT
& READINESS COMMAND
5001 EISENHOWER AVENUE
ALEXANDRIA, VA 22333
ATTN DRXAM-TL, HQ TECH LIBRARY
ATTN DRCDE, DIR FOR DEV & ENGR
ATTN DRCRP-MG, C. M. MCKEEN, JR.
ATTN DRCRP-M, COL R. W. SPECKER
ATTN DRCRD-U, COL J. F. BLEECKER
ATTN DRCRD-F, AIR SYSTEMS DIV
ATTN DRCRD-SI, H. DARRICOTT
ATTN DRCSO, SURVEILLANCE, TARGET ACQ
ATTN DRCMS-I, DR. R. P. UHLIG
ATTN DRCMS-I, MR. E. O'DONNEL

COMMANDER
USA ARMAMENTS COMMAND
ROCK ISLAND, IL 61201
ATTN DRSAR-ASF, FUZE DIV
ATTN DRSAR-RDF, SYS DEV DIV - FUZES
ATTN DRSAR-PDM, J. A. BRINKMAN
ATTN DRCPM-VFF

COMMANDER
USA RSCH & STD GP (EUR)
BOX 65
FPO NEW YORK 09510
ATTN LTC JAMES M. KENNEDY, JR.
CHIEF, PHYSICS & MATH BRANCH

COMMANDER
USA MISSILE & MUNITIONS
CENTER & SCHOOL
REDSTONE ARSENAL, AL 35809
ATTN ATSK-CTD-F

DEFENSE ADVANCED RESEARCH PROJECTS
1400 WILSON BLVD
ARLINGTON, VA 22209
ATTN TECH INFORMATION OFFICE
ATTN DIR, STRATEGIC TECHNOLOGY
ATTN DIR, TACTICAL TECHNOLOGY

DIRECTOR
DEFENSE COMMUNICATION ENG CENTER
1860 WIEHLE AVENUE
RESTON, VA 22070
ATTN R104, M. J. RAFFENSPERGER
ATTN R800, R. E. LYONS

DIRECTOR
DEFENSE INTELLIGENCE AGENCY
WASHINGTON, DC 20301
ATTN DI-2, WEAPONS & SYSTEMS DIV

DIRECTOR
DEFENSE NUCLEAR AGENCY
WASHINGTON, DC 20305
ATTN PETER HAAS, DEP. DIR,
SCIENTIFIC TECHNOLOGY
ATTN RAEV, MAJ S. O. KENNEDY, SR.
ATTN VLIS, LTC SHIMERDA

DEPARTMENT OF DEFENSE
DIRECTOR OF DEFENSE RESEARCH
& ENGINEERING
WASHINGTON, DC 20301
ATTN DEP DIR (TACTICAL WARFARE PROGRAMS)
ATTN DEP DIR (TEST & EVALUATION)
ATTN DEFENSE SCIENCE BOARD
ATTN ASST DIR SALT SUPPORT GP,
MR. J. BLAYLOCK

CHAIRMAN
JOINT CHIEFS OF STAFF
WASHINGTON, DC 20301
ATTN J-3, NUCLEAR WEAPONS BR
ATTN J-3, EXER PLANS & ANALYSIS DIV
ATTN J-5, NUCLEAR DIR NUCLEAR POLICY BR
ATTN J-5, REQUIREMENTS & DEV BR
ATTN J-6, COMMUNICATIONS-ELECTRONICS

DEPARTMENT OF DEFENSE
JOINT CHIEFS OF STAFF
STUDIES ANALYSIS & GAMING AGENCY
WASHINGTON, DC 20301
ATTN STRATEGIC FORCES DIV
ATTN GEN PURPOSE FORCES DIV
ATTN TAC NUC BR
ATTN SYS SUPPORT BR

ASSISTANT SECRETARY OF DEFENSE
PROGRAM ANALYSIS AND EVALUATION
WASHINGTON, DC 20301
ATTN DEP ASST SECY (GEN PURPOSE PROG)
ATTN DEP ASST SECY (REGIONAL PROGRAMS)
ATTN DEP ASST SECY (RESOURCES ANALYSIS)

DEPARTMENT OF THE ARMY
OFFICE, SECRETARY OF THE ARMY
WASHINGTON, DC 20301
ATTN ASST SECRETARY OF THE ARMY (I&L)
ATTN DEP FOR MATERIEL ACQUISITION
ATTN ASST SECRETARY OF THE ARMY (R&D)

DEPARTMENT OF THE ARMY
ASSISTANT CHIEF OF STAFF FOR INTELLIGENCE
WASHINGTON, DC 20301
ATTN DAMI-OC, COL J. A. DODDS
ATTN DAMI-TA, COL F. M. GILBERT

US ARMY SECURITY AGENCY
ARLINGTON HALL STATION
4000 ARLINGTON BLVD
ARLINGTON, VA 22212
ATTN DEP CH OF STAFF RESEARCH & DEVELOPMENT

DISTRIBUTION (Cont'd)

DEPARTMENT OF THE ARMY
US ARMY CONCEPTS ANALYSIS AGENCY
8120 WOODMONT AVENUE
BETHESDA, MD 20014
ATTN COMPUTER SUPPORT DIV
ATTN WAR GAMING DIRECTORATE
ATTN METHODOLOGY AND RESOURCES DIR
ATTN SYS INTEGRATION ANALYSIS DIR
ATTN JOINT AND STRATEGIC FORCES DIR
ATTN FORCE CONCEPTS AND DESIGN DIR
ATTN OPERATIONAL TEST AND EVALUATION AGENCY

DIRECTOR
NATIONAL SECURITY AGENCY
FORT GEORGE G. MEADE, MD 20755

COMMANDER-IN-CHIEF
EUROPEAN COMMAND
APO NEW YORK, NY 09128

HEADQUARTERS
US EUROPEAN COMMAND
APO NEW YORK, NY 09055

DIRECTOR
WEAPONS SYSTEMS EVALUATION GROUP
OFFICE, SECRETARY OF DEFENSE
400 ARMY-NAVY DRIVE
WASHINGTON, DC 20305
ATTN DIR, LT GEN GLENN A. KENT

DEPARTMENT OF THE ARMY
DEPUTY CHIEF OF STAFF FOR
OPERATIONS & PLANS
WASHINGTON, DC 20301
ATTN DAMO-RQZ, LTC L. A. WEIZEL
ATTN DAMO-RQD, COL E. W. SHARP
ATTN DAMO-SSP, COL D. K. LYON
ATTN DAMO-SSN, LTC R. E. LEARD
ATTN DAMO-SSN, LTC B. C. ROBINSON
ATTN DAMO-RQZ, COL G. A. POLLIN, JR.
ATTN DAMO-TCZ, MG T. M. REINZI
ATTN DAMO-ZD, A. GOLUB

DEPARTMENT OF THE ARMY
CHIEF OF RESEARCH DEVELOPMENT
AND ACQUISITION OFFICE
WASHINGTON, DC 20301
ATTN DAMA-RAZ-A, R. J. TRAINOR
ATTN DAMA-CSM-N, LTC OGDEN
ATTN DAMA-WSA, COL W. E. CROUCH, JR.
ATTN DAMA-WSW, COL L. R. BAUMANN
ATTN DAMA-CSC, COL H. C. JELINEK
ATTN DAMA-CSM, COL H. R. BAILEY
ATTN DAMA-WSZ-A, MG D. R. KEITH
ATTN DAMA-WSM, COL J. B. OBLINGER, JR.
ATTN DAMA-PPR, COL D. E. KENNEY

COMMANDER
BALLISTIC MISSILE DEFNSE SYSTEMS
PO BOX 1500
HUNTSVILLE, AL 35807
ATTN BMDSC-TEN, MR. JOHN VEFNEMAN

COMMANDER
US ARMY FOREIGN SCIENCE
AND TECHNOLOGY CENTER
220 SEVENTH ST, NE
CHARLOTTESVILLE, VA 22901

DIRECTOR
US ARMY MATERIEL SYSTEMS ANALYSES ACTIVITY
ABERDEEN PROVING GROUND, MD 21005
ATTN DRXSY-C, DON R. BARTHEL
ATTN DRXSY-T, P. REID

COMMANDER
US ARMY SATELLITE COMMUNICATIONS AGENCY
FT. MONMOUTH, NJ 07703
ATTN LTC HOSMER

DIRECTOR
BALLISTIC RESEARCH LABORATORIES
ABERDEEN PROVING GROUND, MD 21005
ATTN DRXBR-XA, MR. J. MESZARDS

COMMANDER
US ARMY AVIATION SYSTEMS COMMAND
12TH AND SPRUCE STREETS
ST. LOUIS, MO 63160
ATTN DRCPM-AAH, ROBERT HUBBARD

DIRECTOR
EUSTIS DIRECTORATE
US ARMY AIR MOBILITY R&D LABORATORY
FORT EUSTIS, VA 23604
ATTN SAVDL-EU-MOS, MR. S. POCILUYKO
ATTN SAVDL-EU-TAS (TETRACORE)

COMMANDER
2D BDE, 101ST ABN DIV (AASLT)
FORT CAMPBELL, KY 42223
ATTN AFZB-KB-SO, CPT PAUL C. SMITH

COMMANDER
US ARMY ELECTRONICS COMMAND
FT. MONMOUTH, NJ 07703
ATTN PM, ATACS/AMCPM-ATC, LTC DOBBINS
ATTN DRCPM-ATC-TM
ATTN PM, ARTADS/AMCPM-TDS, BG A. CRAWFORD
ATTN DRCPM-TDS-TF, COL D. EMERSON
ATTN DRCPM-TDS-TO
ATTN DRCPM-TDS-FB, LTC A. KIRKPATRICK
ATTN PM, MALOR/AMCPM-MALR, COL W. HARRISON
ATTN PM, NAVCON/AMCPM-NC, COL C. MCDOWELL, JR.
ATTN PM, REMBASS/AMCPM-RBS, COL R. COTTEY, SR.
ATTN DRSEL-TL-IR, MR. R. FREIBERG
ATTN DRSEL-SA, NORMAN MILLSTEIN
ATTN DRSEL-MA-C, J. REAVIS

COMMANDER
US ARMY MISSILE COMMAND
REDSTONE ARSENAL, AL 35809
ATTN DRSMI-FRR, DR. F. GIPSON
ATTN DRCPM-HA, COL DEADWYLER
ATTN DRCPM-LCCX, L. B. SEGGEL (LANCE)
ATTN DRCPM-MD, GENE ASHLEY (SAM-D)
ATTN DRCPM-MP
ATTN DRCPM-PE, COL SKEMP (PERSHING)
ATTN DRCPM-SHO
ATTN DRCPM-TO
ATTN DRSMI-R, RDE & MSL DIRECTORATE

COMMANDER
PICATINNY ARSENAL
DOVER, NJ 07801
ATTN SARPA-ND-V, DANIEL WAXLER

COMMANDER
US ARMY TANK & AUTOMOTIVE COMMAND
WARREN, MI 48090
ATTN DRSI-RHT, MR. P. HASEK
ATTN DRCPM(XM-L), MR. L. WOOLCOT
ATTN DRCPM-GCM-SW, MR. R. SLAUGHTER

PRESIDENT
DA, HA, US ARMY ARMOR AND ENGINEER BOARD
FORT KNOX, KY 40121
ATTN STEBB-MO, MAJ SANZOTERRA

COMMANDER
WHITE SANDS MISSILE RANGE
WHITE SANDS MISSILE RANGE, NM 88002
ATTN STEWS-TE-NT, MARVIN SQUIRES

COMMANDER
TRASANA
SYSTEM ANALYSIS ACTIVITY
WHITE SANDS, NM 88002
ATTN ATAA-TDO, DR. D. COLLIER

COMMANDER
197TH INFANTRY BRIGADE
FORT BENNING, GA 31905
ATTN COL WASIAK

COMMANDER
US ARMY COMMUNICATIONS COMMAND
FORT HUACHUCA, AZ 85613
ATTN ACC-AD-C, H. LASITTER (EMP STUDY GP)

COMMANDER
USA COMBINED ARMS COMBAT
DEVELOPMENTS ACTIVITY
FT. LEVENWORTH, KS 66027
ATTN ATCAC
ATTN ATCACO-SD, LTC L. PACHA
ATTN ATCA/COC, COL HUBBERT
ATTN ATCA-CCM-F, LTC BECKER
ATTN ATSW-TA-E, NUCLEAR STUDY TEAM,
LT D. WILKINS

PROJECT MANAGER
MOBILE ELECTRIC POWER
7500 BACKLICK ROAD
SPRINGFIELD, VA 22150
ATTN DRCPM-MEP

COMMANDER
US ARMY NUCLEAR AGENCY
FT. BLISS, TX 79916
ATTN ATCN-W, COL A. DEVERILL

COMMANDER
US ARMY SIGNAL SCHOOL
FT. GORDON, GA 30905
ATTN AISO-CID, BILL MANNELL
ATTN ATST-CTD-CS,
CAPT G. ALEXANDER (INTACS)
ATTN ATSO-CID-CS, LTC R. LONGSHORE

DIRECTOR
JOINT TACTICAL COMMUNICATIONS OFFICE
FT. MONMOUTH, NJ 07703
ATTN TRI-TAC, NORM BECHTOLD

CHIEF OF NAVAL OPERATIONS
NAVY DEPARTMENT
WASHINGTON, DC 20350
ATTN NOP-932, SYS EFFECTIVENESS DIV,
CAPT E. V. LANEY
ATTN NOP-9860, COMMUNICATIONS BR,
COR L. LAYMAN
ATTN NOP-351, SURFACE WEAPONS BR,
CAPT G. A. MITCHELL
ATTN NOP-622C, ASST FOR NUCLEAR
VULNERABILITY, R. PIACESI

COMMANDER
NAVAL ELECTRONICS SYSTEMS COMMAND, HQ
2511 JEFFERSON DAVIS HIGHWAY
ARLINGTON, VA 20360
ATTN PME-117-21, SANGUINE DIV

HEADQUARTERS, NAVAL MATERIAL COMMAND
STARTEGIC SYSTEMS PROJECTS OFFICE
1931 JEFFERSON DAVIS HIGHWAY
ARLINGTON, VA 20390
ATTN NSP2201, LAUNCHING & HANDLING
BRANCH, BR ENGINEER, P. R. FAUROT
ATTN NSP-230, FIRE CONTROL & GUIDANCE
BRANCH, BR ENGINEER, D. GOLD
ATTN NSP-2701, MISSILE BRANCH,
BR ENGINEER, J. W. FITSENBERGER

COMMANDER
NAVAL SURFACE WEAPONS CENTER
WHITE OAK, MD 20910
ATTN CODE 222, ELECTRONICS &
ELECTROMAGNETICS DIV
ATTN CODE 431, ADVANCED ENGR DIV

DISTRIBUTION (Cont'd)

US AIR FORCE, HEADQUARTERS
DCS, RESEARCH & DEVELOPMENT
WASHINGTON, DC 20330
ATTN DIR OF OPERATIONAL REQUIREMENTS
& DEVELOPMENT PLANS, S/V,
LTC P. T. DUESBERRY

COMMANDER
AF WEAPONS LABORATORY, AFSC
KIRTLAND AFB, NM 87117
ATTN ES, ELECTRONICS DIVISION
ATTN EL, J. DARRAH
ATTN TECHNICAL LIBRARY
ATTN D. I. LAWRY

COMMANDER
AERONAUTICAL SYSTEMS DIVISION, AFSC
WRIGHT-PATTERSON AFB, OH 45433
ATTN ASD/YH, DEPUTY FOR B-1

COMMANDER
HQ SPACE & MISSILE SYSTEMS ORGANIZATION
PO 96960 WORLDWAYS POSTAL CENTER
LOS ANGELES, CA 90009
ATTN S7H, DEFENSE SYSTEMS APPL SPO
ATTN XRT, STRATEGIC SYSTEMS DIV
ATTN SYS, SURVIVABILITY OFC

SPACE AND MISSILE SYSTEMS ORGANIZATION
NORTON AFB, CA 92409
ATTN MMH, HARD ROCK SILO DEVELOPMENT

COMMANDER
AF SPECIAL WEAPONS CENTER, AFSC
KIRTLAND AFB, NM 87117

COMMANDANT
US ARMY COMMAND AND GENERAL STAFF COLLEGE
FORT LEAVENWORTH, KS 66027

COMMANDER
US ARMY COMBAT DEVELOPMENTS EXPERIMENTATION
COMMAND
FORT ORD, CA 93941

COMMANDER
HQ MASSTER
FORT HOOD, TX 76544

COMMANDANT
US ARMY AIR DEFENSE SCHOOL
FORT BLISS, TX 79916
ATTN ATSA-CS

COMMANDANT
US ARMY ARMOR SCHOOL
FORT KNOX, KY 40121
ATTN ATSB-CTD (2 COPIES)

COMMANDER
US ARMY AVIATION CENTER
FORT RUCKER, AL 36350
ATTN ATST-D-MS (2 COPIES)

COMMANDER
US ARMY ORDNANCE CENTER AND SCHOOL
ABERDEEN PROVING GROUND, MD 21005
ATTN USAOC&S
ATTN ATSL-CTD

COMMANDANT
US ARMY SIGNAL SCHOOL
FORT GORDON, GA 30905
ATTN ATSS-CTD (2 COPIES)

COMMANDANT
US ARMY ENGINEER SCHOOL
FORT BELVOIR, VA 22060
ATTN ATSE-CTD (2 COPIES)

COMMANDANT
US ARMY INFANTRY SCHOOL
FORT BENNING, GA 31905
ATTN ATSH-CTD (2 COPIES)

COMMANDER
US ARMY INTELLIGENCE CENTER AND SCHOOL
FORT HUACHUCA, AZ 85613 (2 COPIES)

COMMANDANT
US ARMY FIELD ARTILLERY SCHOOL
FORT SILL, OK 73503
ATTN ATSF-CTD (2 COPIES)

HARRY DIAMOND LABORATORIES
ATTN MCGREGOR, THOMAS, COL, COMMANDER/
FLYER, I.N./LANDIS, P.E./
SOMMER, H./OSWALD, R. B.
ATTN CARTER, W.W., DR., TECHNICAL
DIRECTOR/MARCUS, S.M.
ATTN KIMMEL, S., PAO
ATTN CHIEF, 0021
ATTN CHIEF, 0022
ATTN CHIEF, LAB 100
ATTN CHIEF, LAB 200
ATTN CHIEF, LAB 300
ATTN CHIEF, LAB 400
ATTN CHIEF, LAB 500
ATTN CHIEF, LAB 600
ATTN CHIEF, DIV 700
ATTN CHIEF, DIV 800
ATTN CHIEF, LAB 900
ATTN CHIEF, LAB 1000
ATTN RECORD COPY, BR 041
ATTN HDL LIBRARY (3 COPIES)
ATTN CHAIRMAN, EDITORIAL COMMITTEE
ATTN TECH REPORTS, 013
ATTN PATENT LAW BRANCH, 071
ATTN MCLAUGHLIN, P. W., 741
ATTN LANHAM, C., 0021
ATTN CHIEF, 0024
ATTN CHIEF, 1020 (5 COPIES)
ATTN CHIEF, 1030
ATTN CHIEF, 1040
ATTN CHIEF, 1050